

Interplay between preconditioning and regularization for linear ill-posed problems solved by conjugate gradient. Application to optical flow estimation

Ahmed Chabib, Jean-François Witz, Vincent Magnier, Pierre Gosselet

Univ. Lille, CNRS, Centrale Lille, UMR 9013 - LaMcube -
Laboratoire de Mécanique, Multiphysique, Multiéchelle,
F-59000 Lille, France

June 10, 2024

Abstract.

This paper investigates the possibilities offered by combining regularization and preconditioning by the same symmetric positive semi-definite operator when solving ill-posed problems. We study the question of the stopping criterion, and the possibility offered by Ritz eigen elements for a posteriori filtering of the solution and tuning of Tikhonov's weight. The method is applied as the linear solver for an optical flow estimator and it is coupled with a subspace recycling strategy.

Keywords. regularization; preconditioning; conjugate gradient; Ritz values.

License. Published under CC-by license.

1 Introduction

Ill-posed systems of equations are ominous in mechanics. They are particularly present in identification problems, such as the boundary completion in elasticity [13, 7]. They also appear in methods involving some compact operator, like the Herglotz' transform to build solutions to the Helmholtz problems [14]. Beside issues of existence and uniqueness, ill-posed problems are characterized by the lack of stability between the cause and the effect, in other words small perturbations in the input potentially lead to large modifications of the output.

In this paper, we focus on discrete $n \times n$ linear symmetric positive semi-definite systems of the form $\mathbf{Ax} = \mathbf{b}$, allowing to analyze all properties in terms of the spectrum of \mathbf{A} . Existence and uniqueness are linked to the null-space of \mathbf{A} (strictly zeros eigenvalues) whereas stability is associated with the accumulation of eigenvalues near zero. Indeed, a small contribution of \mathbf{b} in an eigendirection associated with a small eigenvalue of \mathbf{A} has a significant impact on \mathbf{x} . Ill-posed problems thus result in poorly conditioned operators.

Solving such systems amounts to finding a satisfactory treatment to these small eigenvalues: truncation, shift, filtering. Truncation involves disregarding the problematic directions, for example using an eigenvalue decomposition $\mathbf{A} = \sum_{i=1}^n \sigma_i \mathbf{u}_i \mathbf{u}_i^T$ (or more generally a singular value decomposition [9]) and only keeping the part of the matrix associated with eigenvalues larger than a given criterion ε :

$$\mathbf{A}^{-1} \simeq \sum_{i=1}^m \frac{\mathbf{u}_i \mathbf{u}_i^T}{\sigma_i}, \quad \sigma_i > \varepsilon > 0, \quad m < n. \quad (1)$$

Note that this idea is approximately implemented by (non-preconditioned) iterative solvers since they tend to favor the upper part of the spectrum in the first iterations, so that one only needs to stop the solver early enough.

Shift is generally achieved thanks to Tikhonov regularization [18], that can be written as, in its simplest form:

$$\mathbf{A} \simeq \mathbf{A}_\lambda = \mathbf{A} + \lambda \mathbf{I}. \quad (2)$$

In that case $\lambda > 0$ becomes the lower bound of the spectrum of \mathbf{A}_λ . Often, a matrix with more physical sense, acting more locally on the small eigenvalues, is available instead of the identity.

Filtering tries to improve a solution after it was computed using another technique by enforcing some physical properties. For instance, smoothing can be used to recover regularity in a noisy solution.

All these techniques are often controlled by a parameter (ε for the truncation, λ for the regularization, the stopping criterion of an iterative solver. . .) which needs to be tuned in order to find a balance between the information inside the original system and the information brought (or removed) by the treatment. When the accuracy of the data is known, Morozov’s principle [15] provides an objective criterion for choosing the parameter: the correction introduced by the added information should not exceed the noise in the measurement.

When no such data is available, a compromise must be found. Picard’s principle [10] compares the eigenvalues (σ_i) (sorted in decreasing order) and the decomposition of the right-hand side on the eigendirections ($\mathbf{u}_i^T \mathbf{b}$). While eigenvalues decrease less rapidly than their contributions to the right-hand side, the solution remains controlled. The L-curve [11] is a visual aid to find a balance. The solutions for various level of regularization are positioned in a frame (“norm of the residual”, “norm of the solution”). In general large regularization leads to low norm of the solution but high error, whereas small regularization leads to lower level of error but large solutions (highly perturbed). Ideally, some corner exists which realizes a compromise between residual and oscillating solution.

In this paper, we attempt to combine these ideas within a sophisticated solver that offers many useful features: several stopping criteria, filtering of the solution and easy tuning of the regularization. It extends previous work in [7], by exploring the interplay between Tikhonov regularization and preconditioning. This work was initiated in the context of optical flow estimation, even though its scope is much broader. A key element in boosting the algorithm’s capabilities is the ability to quickly solve the regularization operator, which is crucial in optical flow.

The paper is organized as follows. In Section 2, we recall the augmented preconditioned conjugate gradient algorithm and the computation of Ritz eigenelements, providing a first discussion on the effects of the preconditioner. In Section 3, we consider the case of regularized systems preconditioned by the regularization matrix. Section 4 provides assessments based on the optical flow estimation briefly explained in Appendix A. Section 5 concludes the paper.

2 Preconditioned Conjugate Gradient and Ritz elements

We use normal font for scalars, boldface lowercase for vectors and boldface uppercase for matrices. A collection of vectors (\mathbf{x}_j) can be put in the matrix form $\mathbf{X}_m = (\mathbf{x}_0, \dots, \mathbf{x}_{m-1})$, the index m thus corresponds to the number of columns of the matrix. We work in \mathbb{R}^n even though the methods also apply for complex matrices and vectors.

Let \mathbf{A} be a symmetric definite positive matrix and \mathbf{b} be a vector. We search the solution to the system $\mathbf{A}\mathbf{x} = \mathbf{b}$. We use a conjugate gradient, preconditioned by the symmetric positive semi-definite matrix \mathbf{M} , and augmented by the $n \times n_C$ full-rank matrix \mathbf{C} such that $\ker(\mathbf{M}) \subset \text{Range}(\mathbf{C})$.

At iteration i , we note \mathbf{x}_i the approximation and $\mathbf{r}_i = \mathbf{b} - \mathbf{A}\mathbf{x}_i$ the residual. We introduce the augmented Krylov subspace $\mathcal{K}_i(\mathbf{M}^{-1}\mathbf{A}, \mathbf{C}, \mathbf{M}^{-1}\mathbf{r}_0)$ [5]:

$$\mathcal{K}_i(\mathbf{M}^{-1}\mathbf{A}, \mathbf{C}, \mathbf{M}^{-1}\mathbf{r}_0) = \text{span} \left(\mathbf{M}^{-1}\mathbf{r}_0, \dots, (\mathbf{M}^{-1}\mathbf{A})^{(i-1)}\mathbf{M}^{-1}\mathbf{r}_0 \right) \oplus \text{Range}(\mathbf{C}) \quad (3)$$

Given an arbitrary initialization \mathbf{x}_{00} and associated residual $\mathbf{r}_{00} = \mathbf{b} - \mathbf{A}\mathbf{x}_{00}$, the i_{th} iteration can be defined as:

$$\begin{cases} \text{find} & \mathbf{x}_i \in \mathbf{x}_{00} + \mathcal{K}_i(\mathbf{M}^{-1}\mathbf{A}, \mathbf{C}, \mathbf{M}^{-1}\mathbf{r}_{00}) \\ \text{such that} & \mathbf{r}_i \perp \mathcal{K}_i(\mathbf{M}^{-1}\mathbf{A}, \mathbf{C}, \mathbf{M}^{-1}\mathbf{r}_{00}) \end{cases} \quad (4)$$

This iteration is achieved by Algorithm 1 where the augmentation is managed by the correction of the initialization (in order to obtain \mathbf{x}_0) and the projector \mathbf{P} on $\ker(\mathbf{C}^T\mathbf{A})$, which together ensure that the residual remains orthogonal to $\text{Range}(\mathbf{C})$ [6].

Algorithm 1 Augmented Conjugate Gradient

\mathbf{x}_{00} and \mathbf{C} given
 $\mathbf{P} = \mathbf{I} - \mathbf{C}(\mathbf{C}^T\mathbf{A}\mathbf{C})^{-1}\mathbf{C}^T\mathbf{A}$
 $\mathbf{x}_0 = \mathbf{P}\mathbf{x}_{00} + \mathbf{C}(\mathbf{C}^T\mathbf{A}\mathbf{C})^{-1}\mathbf{C}^T\mathbf{b} = \mathbf{x}_{00} + \mathbf{C}(\mathbf{C}^T\mathbf{A}\mathbf{C})^{-1}\mathbf{C}^T\mathbf{r}_{00}$
 $\mathbf{r}_0 = \mathbf{b} - \mathbf{A}\mathbf{x}_0 = \mathbf{P}^T\mathbf{r}_{00}$
 $\mathbf{z}_0 = \mathbf{P}\mathbf{M}^{-1}\mathbf{r}_0, \mathbf{w}_0 = \mathbf{z}_0$
 $\gamma_0 = (\mathbf{z}_0^T\mathbf{r}_0)$
for $i = 0, 1, \dots, m$ (convergence) **do**
 $\mathbf{q}_i = \mathbf{A}\mathbf{w}_i$
 $\delta_i = (\mathbf{w}_i^T\mathbf{q}_i), \alpha_i = \delta_i^{-1}\gamma_i$
 $\mathbf{x}_{i+1} = \mathbf{x}_i + \mathbf{w}_i\alpha_i$
 $\mathbf{r}_{i+1} = \mathbf{r}_i - \mathbf{q}_i\alpha_i$
 $\mathbf{z}_{i+1} = \mathbf{P}\mathbf{M}^{-1}\mathbf{r}_{i+1}$
 $\gamma_{i+1} = (\mathbf{z}_{i+1}^T\mathbf{r}_{i+1})$
 $\beta_i = \gamma_i^{-1}\gamma_{i+1}$
 $\mathbf{w}_{i+1} = \mathbf{z}_{i+1} + \mathbf{w}_i\beta_i$
end for

The algorithm builds two special basis of $\mathcal{K}_i(\mathbf{M}^{-1}\mathbf{A}, \mathbf{C}, \mathbf{M}^{-1}\mathbf{r}_0)$, \mathbf{Z}_i is \mathbf{M} -orthogonal whereas \mathbf{W}_i is \mathbf{A} -orthogonal:

$$\begin{aligned} \mathbf{Z}_i^T\mathbf{M}\mathbf{Z}_i &= \mathbf{Z}_i^T\mathbf{R}_i = \text{diag}(\gamma_j)_{0 \leq j < i} \\ \mathbf{W}_i^T\mathbf{A}\mathbf{W}_i &= \mathbf{W}_i^T\mathbf{Q}_i = \text{diag}(\delta_j)_{0 \leq j < i} \end{aligned} \quad (5)$$

It is convenient to introduce the \mathbf{M} -normalized version of the \mathbf{Z}_i basis:

$$\hat{\mathbf{z}}_i = \frac{(-1)^i\mathbf{z}_i}{\sqrt{\gamma_i}} \quad \text{so that} \quad \hat{\mathbf{Z}}_i^T\mathbf{M}\hat{\mathbf{Z}}_i = \mathbf{I} \quad (6)$$

$\hat{\mathbf{Z}}_i$ is in fact the basis that would have been obtained by the Arnoldi procedure [16], and we have:

$$\begin{aligned} \hat{\mathbf{Z}}_i^T\mathbf{A}\hat{\mathbf{Z}}_i &= \mathbf{T}_i = \text{Tridiag}(\eta_{j-1}, \mu_j, \eta_j) \\ \text{with } \mu_0 &= \frac{1}{\alpha_0}, \quad \mu_j = \frac{1}{\alpha_j} + \frac{\beta_{j-1}}{\alpha_{j-1}}, \quad \eta_j = \frac{\sqrt{\beta_j}}{\alpha_j} \end{aligned} \quad (7)$$

We can diagonalize $\mathbf{T}_i = \mathbf{\Xi}_i\mathbf{\Theta}_i\mathbf{\Xi}_i^T$ where $\mathbf{\Theta}_i$ is the diagonal matrix of eigenvalues sorted in decreasing order and $\mathbf{\Xi}_i$ the orthonormal matrix of eigenvectors.

The Ritz vectors are $\mathbf{V}_i = \hat{\mathbf{Z}}_i\mathbf{\Xi}_i$, while $\mathbf{\Theta}_i$ are the Ritz values of the system. They satisfy:

$$\mathbf{V}_i^T\mathbf{M}\mathbf{V}_i = \mathbf{I} \quad \text{and} \quad \mathbf{V}_i^T\mathbf{A}\mathbf{V}_i = \mathbf{\Theta}_i. \quad (8)$$

In order to mark the dependency of the Ritz vectors and values on the iteration i , they are denoted with an exponent (i) : $\mathbf{\Theta}_i = \text{diag}(\theta_j^{(i)})_{1 \leq j \leq i}$ and $\mathbf{V}_i = (\mathbf{v}_1^{(i)}, \dots, \mathbf{v}_i^{(i)})$. As the number of iterations i increases, the $(\theta_j^{(i)})_{1 \leq j \leq i}$ and $(\mathbf{v}_j^{(i)})_{1 \leq j \leq i}$ tend to approximate the generalized eigenvalues and eigenvectors of the couple (\mathbf{A}, \mathbf{M}) [12].

2.1 Role of the preconditioner

It is often said that the preconditioner should be a good approximation of the inverse of \mathbf{A} , in the sense that the spectrum of $\mathbf{M}^{-1}\mathbf{A}$ should be as concentrated as possible around a non-zero value (which can be scaled to 1). This can be roughly estimated by the condition number of $\mathbf{M}^{-1}\mathbf{A}$, but more sophisticated studies are available [2]. It is important to note the proximity between the conjugate gradient algorithm to solve linear systems and the Lanczos procedure to compute eigenvalues [17], as was made explicit by the Ritz analysis in this section’s introduction. It is also useful to see that the higher part of the spectrum is explored in priority due to the repeated power in the construction of Krylov subspace.

In the case of poorly-conditioned systems, the preconditioner can play a regularization role, as was explored in [7]. Schematically, for a direction \mathbf{d} , what matters is the ratio $(\mathbf{d}^T \mathbf{A} \mathbf{d} / \mathbf{d}^T \mathbf{M} \mathbf{d})$. If the preconditioner measures the irregularity of a field, it penalizes the highly oscillating directions and delays their exploration.

Also, the preconditioner can be viewed as providing a physic-based alternative to the simple Euclidean orthogonality. It thus defines “natural” norms which are useful in the analysis of the iterations, as discussed in next subsection.

2.2 Stopping criteria

Conjugate gradient gives valuable pieces of information at no cost, but in specific norms, in the course of the iterations. First, we have error estimators [1]:

$$\begin{aligned} \|\mathbf{r}_i\|_{\mathbf{M}^{-1}}^2 &= \gamma_i \\ \|\mathbf{x}_{i+1} - \mathbf{x}\|_{\mathbf{A}}^2 &= \|\mathbf{x}_i - \mathbf{x}\|_{\mathbf{A}}^2 - \gamma_i^2 \delta_i^{-1} \end{aligned} \quad (9)$$

of course the difficulty for the second identity is that $\|\mathbf{x}_0 - \mathbf{x}\|_{\mathbf{A}}^2$ is unknown. We also have measurement of the norm of the correction brought by iterations [7]:

$$\begin{aligned} \|\mathbf{x}_{i+1} - \mathbf{x}_0\|_{\mathbf{M}}^2 &= \|\mathbf{x}_i - \mathbf{x}_0\|_{\mathbf{M}}^2 + \alpha_i^2 \|\mathbf{w}_i\|_{\mathbf{M}}^2 + 2\alpha_i (\mathbf{w}_i^T \mathbf{M} (\mathbf{x}_i - \mathbf{x}_0)) \\ \text{with } \begin{cases} \|\mathbf{w}_{i+1}\|_{\mathbf{M}}^2 &= \gamma_i + \beta_i^2 \|\mathbf{w}_i\|_{\mathbf{M}}^2, & \|\mathbf{w}_0\|_{\mathbf{M}}^2 &= \gamma_0, \\ (\mathbf{w}_{i+1}^T \mathbf{M} (\mathbf{x}_{i+1} - \mathbf{x}_0)) &= -\beta_i ((\mathbf{w}_i^T \mathbf{M} (\mathbf{x}_i - \mathbf{x}_0)) + \alpha_i \|\mathbf{w}_i\|_{\mathbf{M}}^2). \end{cases} \end{aligned} \quad (10)$$

Finally, we have an estimator on the preconditioned operator:

$$\begin{aligned} \|\mathbf{T}_0\|_F^2 &= \mu_0^2, \\ \|\mathbf{T}_{i+1}\|_F^2 &= \|\mathbf{T}_i\|_F^2 + \mu_i^2 + \eta_i^2 + \eta_{i-1}^2 \rightarrow \|\mathbf{M}^{-1}\mathbf{A}\|_F^2, \end{aligned} \quad (11)$$

where index F stands for the Frobenius norm, $\|\mathbf{M}^{-1}\mathbf{A}\|_F^2$ is the sum of the squares of the generalized eigenvalues of (\mathbf{A}, \mathbf{M}) .

We can then devise costless stopping criteria:

$$\begin{aligned} \|\mathbf{r}_i\|_{\mathbf{M}^{-1}} &< \varepsilon \|\mathbf{r}_0\|_{\mathbf{M}^{-1}}, \\ \|\mathbf{r}_i\|_{\mathbf{M}^{-1}} &< \varepsilon \|\mathbf{T}_i\|_F \|\mathbf{x}_i - \mathbf{x}_0\|_{\mathbf{M}}. \end{aligned} \quad (12)$$

The first one is very classical, but it is risky in the sense that it may be too strict if the initialization or the augmentation were well-chosen ($\|\mathbf{r}_0\|_{\mathbf{M}^{-1}}$ is already small). The second one is inspired from the Scipy implementation of MinRes with a more adapted choice of norms, we are sorry not to know whom to attribute it to. It is interesting in the sense that it balances the reduction of error and the increase of the norm of the solution, which is always a dilemma when solving ill-posed problems. It is often interesting to combine the criteria, add stagnation detection, and to also use safeguards in absolute value in case of too good initialization and augmentation.

2.3 A posteriori filtering

In the case of a poorly conditioned system, the reduction of the error can be obtained at the price of an explosion of the norm of the solution. This is well explained by Picard analysis: the phenomenon occurs when the eigenvalues of the operator decrease faster than the contribution of the right-hand side in the associated direction. It can also be visualized on a L-curve, in the positive quarter of a frame of the form $(\|\mathbf{r}_i\|, \|\mathbf{x}_{i+1}\|)$: the curve starts in the bottom right corner (large error, small norm) with a fast decay of the error, and finishes in the top left corner (reduced error, large norm).

As shown earlier, conjugate gradient provides natural norms to evaluate the error and the norm of the solution: $\|\mathbf{x}_i - \mathbf{x}\|_{\mathbf{A}}$ and $\|\mathbf{x}_i - \mathbf{x}_0\|_{\mathbf{M}}$. With this choice of norms, the curve is always oriented toward the upper-left corner: at each iteration, the norm of the error decreases and the norm of the solution increases.

Ritz elements offer a convenient way to filter the solution. Assuming m iterations were conducted, we can process the basis \mathbf{V}_m and the values Θ_m . We can decompose the right-hand side on the Ritz basis $r_j^{(m)} = \mathbf{v}_j^{(m)T} \mathbf{r}_0$, and define:

$$\text{for } i \leq m, \quad \tilde{\mathbf{x}}_i^{(m)} = \mathbf{x}_0 + \sum_{j=1}^i \frac{r_j^{(m)}}{\theta_j^{(m)}} \mathbf{v}_j^{(m)}. \quad (13)$$

We have:

$$\begin{aligned} \|\tilde{\mathbf{x}}_i^{(m)} - \mathbf{x}\|_{\mathbf{A}}^2 &= \|\tilde{\mathbf{x}}_i^{(m)} - \mathbf{x}_0\|_{\mathbf{A}}^2 - \sum_{j=1}^i \frac{(r_j^{(m)})^2}{\theta_j^{(m)}}, \\ \|\tilde{\mathbf{x}}_i^{(m)} - \mathbf{x}_0\|_{\mathbf{M}}^2 &= \sum_{j=1}^i \frac{(r_j^{(m)})^2}{(\theta_j^{(m)})^2}, \end{aligned} \quad (14)$$

and of course:

$$\|\tilde{\mathbf{x}}_i^{(m)} - \tilde{\mathbf{x}}_{i-1}^{(m)}\|_{\mathbf{A}}^2 = \frac{(r_i^{(m)})^2}{\theta_i^{(m)}} \quad \text{and} \quad \|\tilde{\mathbf{x}}_i^{(m)} - \tilde{\mathbf{x}}_{i-1}^{(m)}\|_{\mathbf{M}}^2 = \frac{(r_i^{(m)})^2}{(\theta_i^{(m)})^2}. \quad (15)$$

Since the $(\theta_j^{(m)})$ are sorted in decreasing order, we see that the error of $(\tilde{\mathbf{x}}_i^{(m)})$ tends to decrease slower than its norm tends to increase. The L-curve for $(\tilde{\mathbf{x}}_i^{(m)})_i$ is then convex and the corner may be easier to define. The slope of the L-curve between the point $i-1$ and i is $-(\theta_i^{(m)})^{-1}$. A possibility is to define the corner as the point which maximizes the variation of slope: $i = \arg \max_j ((\theta_{j+1}^{(m)})^{-1} - (\theta_j^{(m)})^{-1})$.

Ritz' elements also make it possible to use Picard's theory and stop the construction of $\tilde{\mathbf{x}}_i^{(m)}$ when the contribution $r_j^{(m)}$ starts to decrease less fast than $\theta_j^{(m)}$. This criterion has the advantage to take into account the properties of the right-hand side.

3 Preconditioning by regularization

In general, preconditioning is important because it can speed up the convergence of iterative solvers. As evoked in Section 2, it becomes crucial for ill-posed problem for the physical information it provides and also because the resolution will be stopped "early". Since a too strict convergence criterion can not be attained in a reasonable amount of time, two distinct preconditioners lead to different history of resolution and to qualitatively very different solutions.

We are interested in Tikhonov-regularized systems of the form:

$$\underbrace{(\mathbf{A} + \lambda \mathbf{M})}_{\mathbf{A}_\lambda} \mathbf{x}_\lambda = \underbrace{\mathbf{b}_\mathbf{A} + \lambda \mathbf{b}_\mathbf{M}}_{\mathbf{b}_\lambda} \quad (16)$$

As suggested by the notation, we investigate the effects of using the same operator for the regularization and the preconditioning, in particular when there exists a cheap technique to apply the preconditioner (i.e. \mathbf{M}^{-1}). Conceptually, this idea makes sense as the same physical motivation underlies the choice of the regularization and that of the preconditioner. Moreover, many opportunities are opened by this choice.

If we assume that the system (16) was solved for a given λ in m iterations, then we can process the Ritz basis \mathbf{V}_m . The strong point is that the properties of \mathbf{V}_m are independent of λ :

$$\begin{aligned}\mathbf{V}_m^T \mathbf{M} \mathbf{V}_m &= \mathbf{I} \\ \mathbf{V}_m^T \mathbf{A}_\lambda \mathbf{V}_m &= \Theta_{\lambda,m} = \Theta_m + \lambda \mathbf{I}.\end{aligned}\tag{17}$$

Remark 1. λ can be viewed as a shift in the generalized eigenvalues of (\mathbf{A}, \mathbf{M}) . Since λ alters the initial residual and only a limited number of iterations is made, the content of \mathbf{V}_m is influenced by λ , without impairing the orthogonality properties.

Note that the initial residual takes the form:

$$\mathbf{r}_{\lambda,0} = \mathbf{b}_\lambda - \mathbf{A}_\lambda \mathbf{x}_0 = \underbrace{(\mathbf{b}_\mathbf{A} - \mathbf{A} \mathbf{x}_0)}_{\mathbf{r}_{\mathbf{A},0}} + \lambda \underbrace{(\mathbf{b}_\mathbf{M} - \mathbf{M} \mathbf{x}_0)}_{\mathbf{r}_{\mathbf{M},0}}\tag{18}$$

After m iterations, we can define the Ritz' approximation:

$$\tilde{\mathbf{x}}_{\lambda,i}^{(m)} = \mathbf{x}_0 + \sum_{j=1}^i \mathbf{v}_j^{(m)} \frac{(\mathbf{v}_j^{(m)})^T \mathbf{r}_{\lambda,0}}{\theta_j^{(m)} + \lambda} = \mathbf{x}_0 + \sum_{j=1}^i \mathbf{v}_j^{(m)} \frac{\mathbf{v}_j^{(m)T} \mathbf{r}_{\mathbf{A},0} + \lambda \mathbf{v}_j^{(m)T} \mathbf{r}_{\mathbf{M},0}}{\theta_j^{(m)} + \lambda}\tag{19}$$

This approximation can be computed at zero cost, and its dependence in λ is explicit: the L-curve of $\lambda \mapsto \tilde{\mathbf{x}}_{\lambda,i}^{(m)}$ can be plotted as a continuous function. It even permits to give sense to the limit solution when $\lambda \rightarrow 0$ even when \mathbf{A} was not invertible. It also gives an analytical formula for the search of the optimal choice of (λ, i) realizing a good compromise between error and norm of the solution. Indeed, noting $r_{\lambda,j}^{(m)} = \mathbf{v}_j^{(m)T} \mathbf{r}_{\lambda,0}$, we have the properties:

$$\begin{aligned}\|\tilde{\mathbf{x}}_{\lambda,i}^{(m)} - \mathbf{x}_0\|_{\mathbf{M}}^2 &= \sum_{j=1}^i \left(\frac{r_{\lambda,j}^{(m)}}{\theta_j^{(m)} + \lambda} \right)^2 \\ \|\tilde{\mathbf{x}}_{\lambda,i}^{(m)} - \mathbf{x}_\lambda\|_{\mathbf{A}_\lambda}^2 &= \mathbf{r}_{\lambda,0}^T (\mathbf{A} + \lambda \mathbf{M})^{-1} \mathbf{r}_{\lambda,0} - \frac{(r_{\lambda,j}^{(m)})^2}{\theta_j^{(m)} + \lambda}\end{aligned}\tag{20}$$

Sadly, the measurement of the error in a λ -independent norm like $\|\tilde{\mathbf{x}}_{\lambda,i}^{(m)} - \mathbf{x}_\lambda\|_{\mathbf{A}}^2$ seems to be unavailable at the moment.

4 Assessments – Application to optical flow reconstruction

The recovery of the optical flow is briefly summarized in Appendix A. It is in fact a nonlinear minimization problem. A pyramidal approach is developed as often in image correlation, in order to provide a meaningful initialization [4]. For simplicity, we focus on the last nonlinear system to be solved, associated with the full image. Anyhow, the initialization of this system was impacted by the choice of the regularization.

We consider the solution to system (23, 24) with augmented preconditioned conjugate gradient, Algorithm 1. Due to the rectangular shape of the images, there exists an extremely cheap way to solve the preconditioner, which is a Laplace operator, using Fast Fourier transform or more precisely discrete cosine transform, see Appendix B.

The proposed test case is a holed composite plate in traction, with a 45° crack to be identified at the bottom of the hole. The speckle in the initial configuration is shown in Figure 1. To quantify the bad conditioning, the non-zero eigenvalues of \mathbf{A} are in the interval $[10^{-6}, 10^2]$.

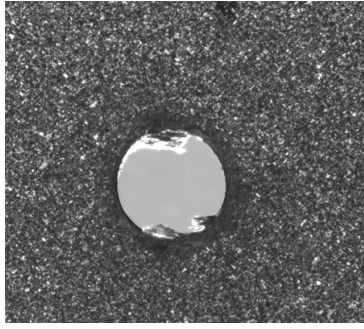


Figure 1: Speckle of the test specimen.

4.1 Quality of the preconditioner

We first wish to verify that preconditioning by regularization actually leads to better enforcement of the regularity. In Table 1, we can qualitatively compare the classical Jacobi approach of preconditioning by the diagonal of the operator $\mathbf{M}_{jac}^{-1} = \text{diag}(\mathbf{A}_\lambda)^{-1}$ and the proposed preconditioning by regularization. The increased regularity is particularly visible for low weight λ and low precision ε of the linear solver.

Preconditioning by the regularization operator thus makes it possible to make meaningful computations with low weight in the regularization and to solve with less precision, hence with fewer iterations. Nevertheless, one has to mention that our preconditioner is computationally more expensive per iteration than the diagonal one.

An interesting scenario unfolds. The regularization preconditioner promotes low frequency corrections. Indeed, it is associated with a fully populated matrix (never actually computed) and the search directions have naturally large wavelength. As iterations progress, higher frequency modes emerge introducing more and more details and irregularity. On the contrary, the Jacobi preconditioner is diagonal, and it naturally encourages (independent) details, only iterations make it possible to reveal the structure between neighboring pixels.

4.2 Ritz filtering

We analyze the solving process for high ($\lambda = 1000$) and low ($\lambda = 10$) levels of regularization. We use the second stopping criterion of Equation 12 with $\varepsilon = 10^{-5}$, which corresponds to a rather high degree of convergence. The identified strain field are given in Figure 4.

We analyze the convergence in terms of compromise between the decrease of the error and the increase of the norm of the gradient of the solution which stems from the oscillations in the identified fields. Figure 2 presents two L-curves associated with high and low regularization. We use the natural CG-norms, please note that the position of the 0-abscissa is conventional because $\|\mathbf{x}_0 - \mathbf{x}\|_{\mathbf{A}}$ is unknown. The L-curves of the CG iterations (dotted lines) have similar shapes, like pieces of hyperbola. Due to the difference of magnitude, different scales had to be used: the error decreases four times less when the high regularization is used, and the norm of the solution remains 50 times smaller.

In order to better understand the convergence, we conduct a Ritz analysis. For $\lambda = 1000$, the convergence is attained in $m = 56$ iterations and as many Ritz vectors are computed. Table 2 presents a selection of these modes, sorted in decreasing order of Ritz value. The Ritz vectors resemble vibration modes with increasing number of anti-nodes. The first vectors are so regular that the hole is barely visible. The crack is only visible on the latest modes. This is bad (but logical) news because these are the most difficult modes to converge, thus they are probably bad approximations of actual eigenmodes, and the crucial mechanical information they carry is difficult to reuse.

We use formula (19) for the *a posteriori* filtering of the solution based on Ritz vectors. We present the L-curves in terms of modes included in the reconstruction. We show the curves in terms of full error and only taking into account the image error ($\mathbf{v}_i^T \mathbf{r}_{\mathbf{A},0}$) — they are almost overlaid on each other, a slight discrepancy only appears for high regularization. The shape

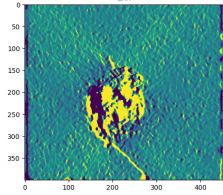
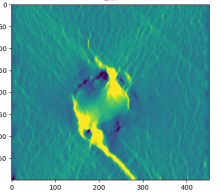
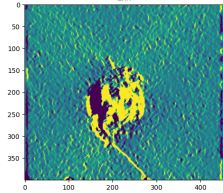
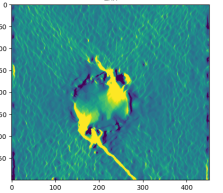
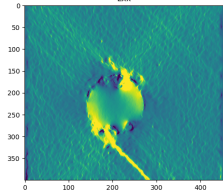
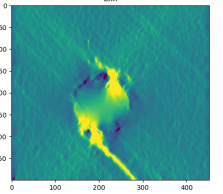
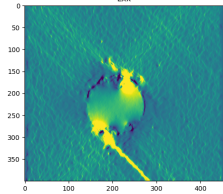
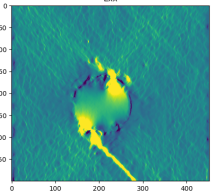
λ	ε	Diagonal Prec.	Regularization Prec.
low	low		
low	high		
high	low		
high	high		

Table 1: ϵ_{xx} strain field (range = mean value \pm 3 st.dev.). Comparison of the effect of preconditioning by diagonal (simple approach) vs by regularization, for different weights $\lambda \in \{1, 1000\}$ and linear solver precision $\varepsilon \in \{10^{-2}, 10^{-3}\}$.

of the Ritz L-curves corresponds to most of the modes (the highest) only slightly decreasing the error and almost not changing the norm, only the last modes, which contain the crack information, are associated with significant decrease of the error (but of course at the cost of much increased solution norm). More or less, if a corner was to be selected it would correspond to just suppressing the contribution of the last mode.

In order to better understand this behavior, we first analyze the convergence of the Ritz values by comparing the spectrum obtained at the last iteration with the one obtained just one iteration before, like was done in [8] in the case of a well posed problem. It appears that the largest Ritz values were quite well approximated and only the lowest part of the spectrum evolves (remember the Ritz values correspond to the inverse of the slope of the segments in the L-curve). In other words, even though the last iterations seem not to modify the solution much (accumulation of the dots in the upper left part on the CG L-curves), they play an important role in terms of estimation of the lower part of the spectrum, without adding lots of small eigenvalues.

To support this analysis, we conduct a Picard's study on Figure 3 which shows the distribution of the Ritz values ($\theta_i^{(m)}$) as well as the decomposition of the right-hand side on the eigenspace ($\mathbf{v}_i^{(m)T} \mathbf{r}_{\mathbf{A},0}$) and $\lambda(\mathbf{v}_i^{(m)T} \mathbf{r}_{\mathbf{M},0})$. It is worth recalling that low and highly regularized systems have the same spectrum, except that it is more sampled for the low regularization which requires two times more iterations to converge. The Ritz values are slowly decreasing and only the last 10% really decay, the low regularization is not associated with an overpopulation of the lowest part of the spectrum. What stands out is the fact that the right-hand side contributes almost equally on all modes (at least it does not decrease for larger Ritz values). Picard's theory

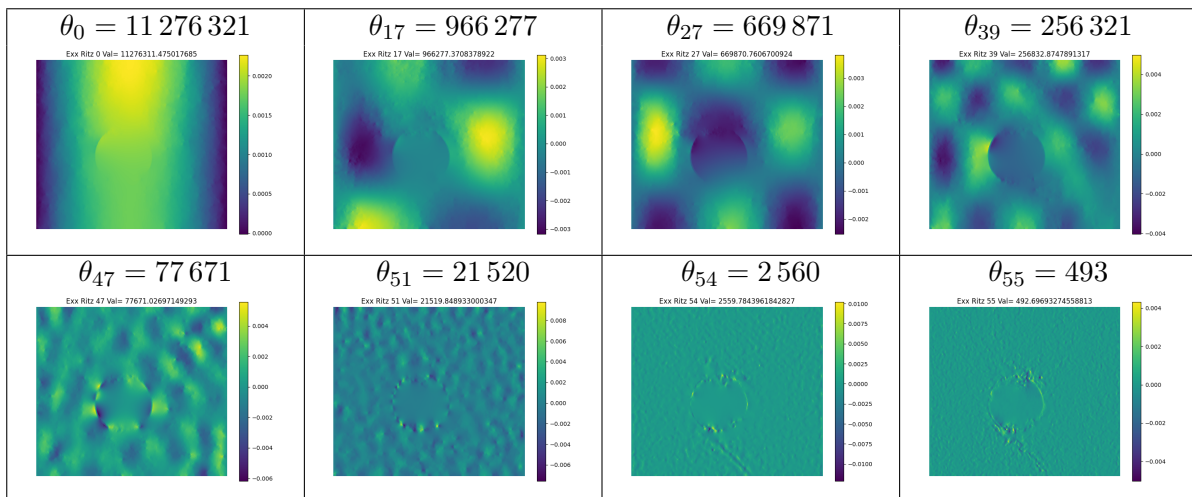


Table 2: ϵ_{xx} strain field for 8 Ritz vectors out of the 56 computed ($\epsilon = 10^{-5}$, $\lambda = 1000$).

thus suggests that we should stop the reconstruction when the Ritz values start to decay. This is not possible in our case since the crack is mostly represented in this part of the spectrum.

By the way, Figure 3 permits to compare the smallest Ritz value θ_{\min} with the regularization parameter λ . The case that we called “low regularization” corresponds to λ being negligible with respect to the small Ritz value $\theta_m^{(m)}$, and thus only marginally modifying the active Ritz spectrum. On the contrary, the high regularization corresponds to a $\lambda > \theta_m^{(m)}$ which means that the lower part of the spectrum of \mathbf{A}_λ is flattened relative to that of \mathbf{A} .

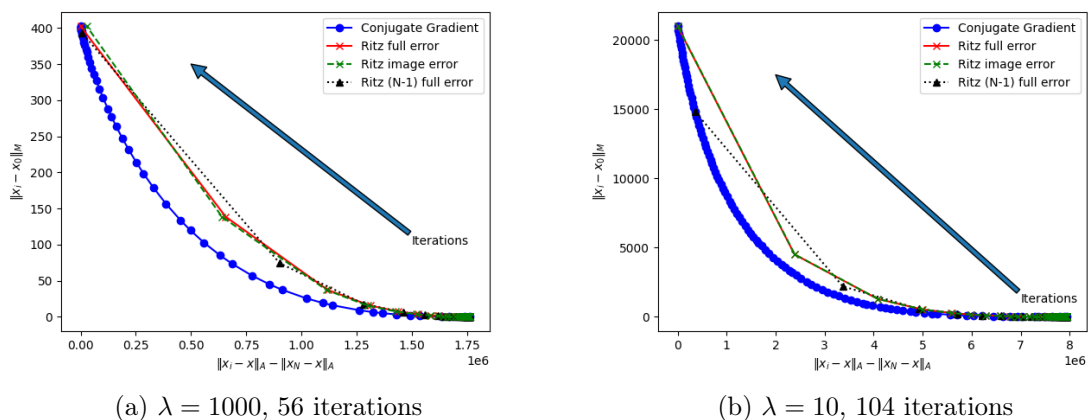


Figure 2: L-curves (same $\epsilon = 10^{-5}$) compared with Ritz post-treatment, for different regularization intensity λ . Note that different scales are used on the plots.

4.3 Subspace recycling

Even though it appears that Ritz filtering is difficult to apply to the studied system, we can still benefit from Ritz vectors to accelerate the solution. As a sequence of linear systems with identical matrix has to be solved, it is natural to augment the system with the previously generated Ritz vectors by concatenating $\mathbf{C} \leftarrow (\mathbf{C} \ \mathbf{V}_m)$. Indeed, augmentation comes with optimized block operations that make augmenting by one vector much cheaper than one iteration.

Moreover, Ritz vectors possess two advantages. Firstly, the product $\mathbf{A}\mathbf{V}_m$ which is required during augmentation can be obtained at low computational cost using the formula: $\mathbf{A}\hat{\mathbf{z}}_{j+1} = (-1)^{j+1}(\mathbf{q}_{j+1} - \beta_j \mathbf{q}_j) / \sqrt{\gamma_{j+1}}$ and $\mathbf{A}\mathbf{V}_m = \mathbf{A}\hat{\mathbf{Z}}_m \mathbf{\Xi}_m$. Secondly, using normalization $\mathbf{V}_m \leftarrow \mathbf{V}_m \mathbf{\Theta}_m^{-1/2}$, we have $\mathbf{V}_m^T \mathbf{A} \mathbf{V}_m = \mathbf{I}$.

Table 3 illustrates the performance of recycling for the nonlinear system to be solved on the

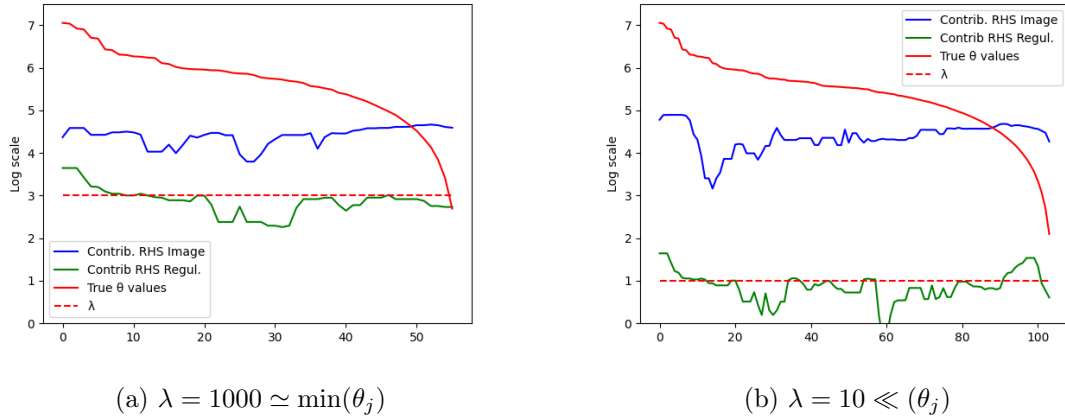


Figure 3: Spectral analysis of the system for $\varepsilon = 10^{-5}$ and different regularization intensity λ . A 5-width median filter was used to smooth out the contribution curves.

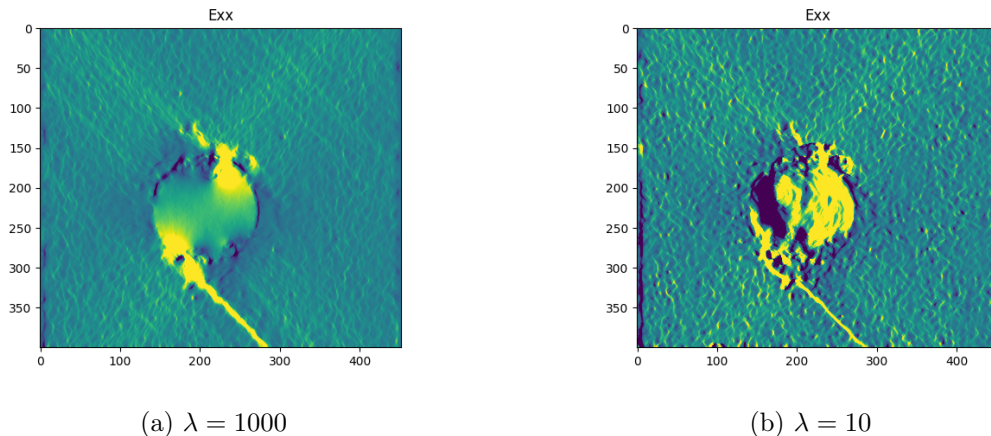


Figure 4: Identified ε_{xx} field, for different regularization intensity λ , with $\varepsilon = 10^{-5}$.

full image at the end of identification. The first linear system, only augmented by the kernel of the preconditioner is solved in 77 iterations. Then a certain portion of the Ritz vectors is used to augment the next 8 linear systems (same matrix, different right-hand sides). As the augmentation results in an excellent initialization, we use a criterion in terms of absolute value of $\|\mathbf{r}_j\|_{\mathbf{M}}$ to halt the iterations because other comparison as given in Equation 12 might use an unfair reference. We measure the performance in terms of gain in iterations, and in computational time (measures are conducted on a upper mid-range laptop with Nvidia RTX A2000 graphic card). The gain in terms of iterations is moderate, with best obtained for small augmentation space (at most 1.3 iterations per augmentation vector, for 10 vectors). In terms of time, the optimal is obtained for augmentation space of 80%-90% of available vectors, with a global CPU time divided by almost 2 (this time includes all the extra cost associated with computing and using Ritz vectors). This size of subspace agrees with what we observed on the stability of the largest Ritz values in the L-curves plots.

4.4 Tuning of λ

It is often hard to automatize the selection of the regularization intensity λ . Picard's plots like in Figure 3 permit to put λ in relation with the spectrum of the preconditioned operator and thus to understand the effect of the regularization in terms of flattened spectrum. Still, the final judge is often the expert's impression of a strain map, and it is convenient to compute maps associated with several (λ_k) at low cost.

Formula (19) makes it possible, after the solution of one linear system for a given λ_0 , to post-

Aug.	0	10	20	30	40	50	60	70	max (77)
Iter.	77	64	57	49	44	41	40	40	38
Time (s)	11.7	10.1	8.3	7.1	6.6	6.3	6.2	6.3	6.6

Table 3: Performance of recycling

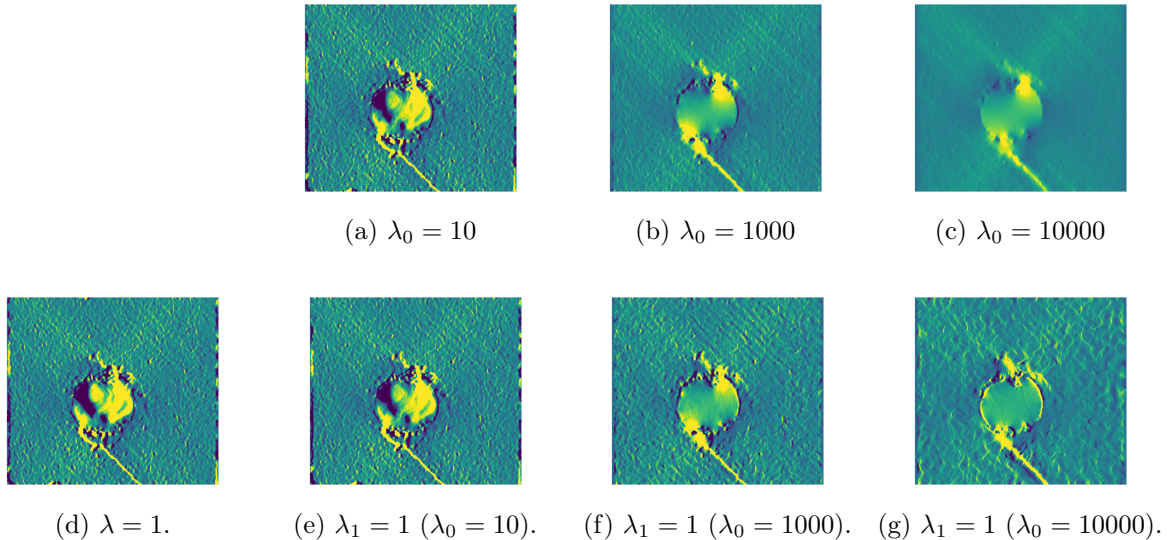


Figure 5: Costless postprocessing for different (λ_i) : top, initial computation with $\lambda_0 \in \{10, 100, 1000\}$; bottom, direct solution with $\lambda = 1$ and solutions deduced with $\lambda_1 = 1$. ϵ_{xx} strain field.

process the solution for any λ_k at the simple cost of computing the associated right-hand side $\mathbf{b}_{\mathbf{A}_{\lambda_k}}$ (which depends on the history of the nonlinear solution for λ_k), and basic linear algebra operations.

Figure 5 presents the solution deduced for $\lambda_1 = 1$ from initial computations with different λ_0 (in $\{10, 1000, 10000\}$) and $\varepsilon = 10^{-4}$. Again, a median filter was applied after the Ritz reconstruction. It seems that the Ritz vectors make it possible to postprocess a reasonable solution with a $\lambda_1 \simeq \lambda_0/1000$. The reconstructed strain field appears to be much less smooth than the original computation (with λ_0) while less noisy than the direct low-regularization computation with $\lambda = 1$. If the deduced solution is not fully satisfying, it can still be used as an excellent initialization for a regular computation.

5 Conclusion

In this paper, we have studied how preconditioning and Tikhonov regularization could be efficiently combined in an augmented preconditioned conjugate gradient. We have shown that this association makes sense from a physical point of view and it made it possible to combine filtering, recycling of subspaces, and postprocessing of all regularized solutions at zero cost. This gives a favorable framework to apply criteria like the L-curve or Picard's analysis.

The solver was applied to a problem of optical flow reconstruction which introduced the extra difficulty of nonlinearity and the fact that the most important information was buried in the lower part of the spectrum. Satisfying results were obtained on actual measurements from digital image correlation of a mechanical test. Postprocessed solutions at zero-cost were still relevant for regularization weight λ divided by up to 1000.

An obvious next step for this work is to consider inexact preconditioners, that is to say when the \mathbf{M}^{-1} matrix in the preconditioning step of the algorithm is only an approximation of the inverse of the regularization matrix \mathbf{M} in the operator. This would make the method applicable on a much broader class of problems.

References

- [1] Owe Axelsson and Igor Kaporin. Error norm estimation and stopping criteria in preconditioned conjugate gradient iterations. *Numerical Linear Algebra with Applications*, 8(4):265–286, 2001.
- [2] Owe Axelsson and Gunhild Lindskog. On the rate of convergence of the preconditioned conjugate gradient method. *Numerische Mathematik*, 48:499–523, 1986.
- [3] Gilles Besnard, François Hild, and Stéphane Roux. Finite-element displacement fields analysis from digital images: application to portevin-le châtelier bands. *Experimental Mechanics*, 46:789–804, 2006.
- [4] Ahmed Chabib, Jean-François Witz, Pierre Gosselet, and Vincent Magnier. The impact of metrics in mechanical imaging. *preprint*, 2023.
- [5] Andrew Chapman and Youssef Saad. Deflated and augmented Krylov subspace techniques. *Numerical Linear Algebra with Applications*, 4(1):43–66, 1997.
- [6] Zdeněk Dostál. Conjugate gradient method with preconditioning by projector. *International Journal of Computer Mathematics*, 23:315–323, 1988.
- [7] Renaud Ferrier, Mohamed L. Kadri, and Pierre Gosselet. The Steklov-Poincaré technique for data completion: Preconditioning and filtering. *International Journal for Numerical Methods in Engineering*, 116(4):270–286, 2018.
- [8] Pierre Gosselet, Christian Rey, and Julien Pebrel. Total and selective reuse of Krylov subspaces for the resolution of sequences of nonlinear structural problems. *International Journal for Numerical Methods in Engineering*, 94(1):60–83, 2013.
- [9] Per Christian Hansen. The truncated SVD as a method for regularization. *BIT Numerical Mathematics*, 27(4):534–553, 1987.
- [10] Per Christian Hansen. The discrete Picard condition for discrete ill-posed problems. *BIT Numerical Mathematics*, 30(4):658–672, 1990.
- [11] Per Christian Hansen. Analysis of discrete ill-posed problems by means of the L-curve. *SIAM review*, 34(4):561–580, 1992.
- [12] Zhongxiao Jia and G.W. Stewart. On the convergence of the Ritz values, Ritz vectors and refined Ritz vectors. Technical Report 3896, Institute of Advanced Computer Studies, Department of Computer Science, University of Maryland at College Park, 1999.
- [13] Mohamed Larbi Kadri, Jalel Ben Abdallah, and Thouraya Nouri Baranger. Identification of internal cracks in a three-dimensional solid body via Steklov–Poincaré approaches. *Comptes Rendus Mécanique*, 339(10):674–681, 2011.
- [14] Louis Kovalevsky and Pierre Gosselet. A quasi-optimal coarse problem and an augmented Krylov solver for the Variational Theory of Complex Rays. *International Journal for Numerical Methods in Engineering*, 2015.
- [15] Vladimir Alekseevich Morozov. The error principle in the solution of operational equations by the regularization method. *Zhurnal Vychislitel’noi Matematiki i Matematicheskoi Fiziki*, 8(2):295–309, 1968.
- [16] Yousef Saad. *Iterative methods for sparse linear systems*. SIAM, 2003.
- [17] Yousef Saad. *Numerical Methods for Large Eigenvalue Problems*, volume 66 of *Classics in Applied Mathematics*. SIAM, Philadelphia, USA, revised edition, 2011.
- [18] Andreï Nikolaevich Tikhonov and Vasilii Iakovlevich Arsenin. *Solutions of ill-posed problems*. Vh Winston, 1977.

A Basic notions about the optical flow

The optical flow is a digital image correlation technique which aims at estimating the displacement field between two images at the scale of the pixel. Contrarily to very popular approaches in solid mechanics inspired by the Finite Element Method [3], it does not rely on a mesh and on shape functions to approximate the displacement field. Given a sequence of two images (I_1, I_2) , viewed as $N \times M$ arrays of gray level pixels (in the discrete segment $\{0, 1, \dots, G_{max}\}$), it directly aims at finding the transformation $\phi = (\phi_x, \phi_y)$ such that $I_1 - I_2 \circ \phi = 0$. Note that we use interpolation between pixels so that the images can be defined on the rectangle $[0, N] \times [0, M] \subset \mathbb{R}^2$ with values in the continuous segment $[0, G_{max}] \subset \mathbb{R}$ and the displacement $u := (\phi - I_d)$ can take non-integer values (I_d is the identity operator). It is even common to obtain precision below one tenth of a pixel. In order to gain flexibility, and adapt to unavoidable noisy measurements which make the zero unachievable, the problem is better rephrased in terms of the minimization of the “image energy” E_I :

$$E_I^2 = \frac{1}{2} \|I_1 - I_2 \circ \phi\|^2, \quad \text{where } \|I\|^2 = \sum_{\substack{0 \leq i < N \\ 0 \leq j < M}} I(i, j)^2. \quad (21)$$

Even under that form the problem is not well-posed, would it only be because there are two times more unknowns than equations. A solution to recover a well-posed problem is to enforce regularity to the displacement field. A penalty term related to the gradient is then introduced:

$$E^2 = E_I^2 + \frac{\lambda}{2} \|\nabla u\|^2, \quad (22)$$

where we kept the Euclidean norm notation for $\|\nabla u\|^2 := \|\partial_x u_x\|^2 + \|\partial_y u_y\|^2 + \|\partial_x u_y\|^2 + \|\partial_y u_x\|^2$. λ is a weight that needs to be tuned in order to balance the contributions of the image energy and of the regularization.

In general, a modified Newton approach is used to minimize the energy. Starting from a guess u , the update $u + du$ is computed by solving the system:

$$(\mathbf{A} + \lambda \mathbf{M})\mathbf{x} = \mathbf{b}_\mathbf{A} + \lambda \mathbf{b}_\mathbf{M}, \quad (23)$$

with

$$\begin{aligned} \mathbf{A} &= \begin{pmatrix} \mathbf{J}_x & \\ & \mathbf{J}_y \end{pmatrix} \begin{pmatrix} \mathbf{I} & \mathbf{I} \\ \mathbf{I} & \mathbf{I} \end{pmatrix} \begin{pmatrix} \mathbf{J}_x & \\ & \mathbf{J}_y \end{pmatrix}, & \mathbf{M} &= \begin{pmatrix} \mathbf{\Delta} & \\ & \mathbf{\Delta} \end{pmatrix} \\ \mathbf{x} &= \begin{pmatrix} \text{vec}(du_x) \\ \text{vec}(du_y) \end{pmatrix}, & \mathbf{b}_\mathbf{A} &= \begin{pmatrix} \text{vec}((I_1 - I_2 \circ \phi)J_x) \\ \text{vec}((I_1 - I_2 \circ \phi)J_y) \end{pmatrix}, & \mathbf{b}_\mathbf{M} &= \begin{pmatrix} \text{vec}(\Delta u_x) \\ \text{vec}(\Delta u_y) \end{pmatrix}. \end{aligned} \quad (24)$$

The vec operator converts images to vectors ($N \times M$ array to NM vector). For $z \in \{x, y\}$, J_z is the z component of the gradient of I_1 , Δu_z is the (scalar) Laplace operator applied to u_z . \mathbf{J}_z is the NM diagonal operator containing the values of the gradient J_z . \mathbf{I} and $\mathbf{\Delta}$ are respectively the NM identity matrix and the NM matrix version of Laplace operator (with Neumann boundary conditions). All the operators are in fact obtained by discrete difference on the image. Note that the gradient of I_1 is used to approximate the current Jacobian. As commonly done in image treatment, a median filter is applied to all the computed increments in order to remove outliers caused by the imperfect speckle.

It is extremely simple to work with \mathbf{A} and \mathbf{M} without assembling them, one only needs to compute and store the two $N \times M$ images $(\mathbf{J}_x, \mathbf{J}_y)$ and use Hadamard product and Laplace function when computing matrix-vector multiplication.

The system is of dimension $2MN$. As said earlier, \mathbf{A} is strongly deficient since its rank is at most MN , a first part of its kernel has the following basis:

$$\text{span} \begin{pmatrix} \mathbf{J}_y \\ -\mathbf{J}_x \end{pmatrix} \subset \ker(\mathbf{A}). \quad (25)$$

The rest of the spectrum is easy to compute since:

$$\mathbf{A} \begin{pmatrix} \mathbf{J}_x \\ \mathbf{J}_y \end{pmatrix} = \begin{pmatrix} \mathbf{J}_x \\ \mathbf{J}_y \end{pmatrix} (\mathbf{J}_x^2 + \mathbf{J}_y^2). \quad (26)$$

The other eigenvalues thus correspond to the square of the norm of the gradient of the image. Pixels where the gradient is zero (bad speckles) are also associated with zero eigenvalues.

\mathbf{M} is also rank deficient, the dimension of its kernel is 2, a basis of its null space is well known:

$$\ker(\mathbf{M}) = \text{span} \begin{pmatrix} \mathbf{1} & 0 \\ 0 & \mathbf{1} \end{pmatrix}, \quad (27)$$

where $\mathbf{1}$ is the vector filled with 1: the kernel of the scalar Laplace operator consists of constant functions. In fact a more efficient basis can be computed at a very low cost:

$$\mathbf{C} = \begin{pmatrix} \frac{\mathbf{1}}{\sqrt{s_{xx}}} & -\mathbf{1} \frac{s_{xy}s_b}{s_{xx}} \\ 0 & s_b \mathbf{1} \end{pmatrix} \text{ with } \begin{cases} s_{xx} = \mathbf{1}^T \mathbf{J}_x^2 \mathbf{1} \\ s_{xy} = \mathbf{1}^T \mathbf{J}_x \mathbf{J}_y \mathbf{1} \\ s_{yy} = \mathbf{1}^T \mathbf{J}_y^2 \mathbf{1} \\ s_b = 1/\sqrt{s_{yy} - s_{xy}^2/s_{xx}} \end{cases} \quad (28)$$

It has the advantage to make the matrix $(\mathbf{C}^T(\mathbf{A} + \lambda\mathbf{M})\mathbf{C}) = (\mathbf{C}^T \mathbf{A} \mathbf{C}) = \mathbf{I}$ for any λ .

B Inverse of Laplacian on a rectangle with Neumann boundary condition

It is well known that plane waves $x \mapsto e^{i\omega \cdot x}$, with $\omega \in \mathbb{R}^2$, form a set of eigenfunctions for the Laplace operator in \mathbb{R}^2 with eigenvalues $-\|\omega\|^2$ (using the Euclidean norm). This can be equivalently formulated by saying that the Fourier transform diagonalizes the Laplacian. Hence, the powerful solution technique (in that case ω is the variable in the Fourier domain):

$$\begin{aligned} \Delta u + f &= 0 && \text{in } \mathbb{R}^2 \\ u &= \mathcal{F}^{-1} \left(\frac{\mathcal{F}(f)}{\|\omega\|^2} \right) \end{aligned} \quad (29)$$

What is remarkable is that the eigenvectors are preserved by discretization. For instance, if we consider the classical 5-point stencil on a unit grid:

$$(\Delta_h u)(x_1, x_2) = u(x_1 + 1, x_2) + u(x_1 - 1, x_2) + u(x_1, x_2 + 1) + u(x_1, x_2 - 1) - 4u(x_1, x_2) \quad (30)$$

and one can check that

$$(\Delta_h e^{i\omega \cdot x})(x_1, x_2) = \underbrace{e^{i(x_1\omega_1 + x_2\omega_2)}}_{e^{i\omega \cdot x}} (e^{i\omega_1} + e^{-i\omega_1} + e^{i\omega_2} + e^{-i\omega_2} - 4) \quad (31)$$

Now, considering a rectangular domain, the boundedness of the domain and the boundary conditions lead to selecting only certain eigenvalues, and eigenvectors are made out of a good combination of plane waves. Consider the unit square $[0, 1]^2$, the eigenvalues $\lambda_{n,m}$ and eigenvectors $v_{n,m}$ of the Laplacian with (homogeneous) Neumann boundary conditions are given by:

$$\begin{aligned} v_{n,m}(k, l) &= \cos\left(\frac{ml\pi}{M}\right) \cos\left(\frac{nk\pi}{N}\right) \\ \lambda_{n,m} &= 2 \left(1 - \cos\left(\frac{n\pi}{N}\right)\right) + 2 \left(1 - \cos\left(\frac{m\pi}{M}\right)\right) \end{aligned} \quad (32)$$

As eigenvectors are cosine functions, the specialization of the Fourier transform to this case takes the name of discrete cosine transform (DCT).

One just needs to take some care of the eigenvalue $\lambda_{0,0} = 0$, associated with the constant eigenvector. The classical solution is to work on functions with zero mean value and nullify the constant term in the transformed function.

We give the python code for the inverse of the discrete Laplacian on a rectangle with Neumann boundary conditions. This discrete Laplace operator can be directly invoked by the `laplace()` function from `scipy.ndimage` with default arguments (`border='reflect'`).

```

import numpy as np
from scipy.fftpack import dctn ,idctn

# Prepare transform of Laplacian for (N,M) images
mwx = 2 * (np.cos(np.pi*np.arange(0,N)/N)-1)
mwy = 2 * (np.cos(np.pi*np.arange(0,M)/M)-1)
[MWX, MWY] = np.meshgrid(mwx, mwy, indexing='ij')
MW = MWX + MWY
MW[0,0] = 1.
iMW = 1. / MW
iMW[0,0] = 0

def SolveLaplaceNeumann(U,iMW): # U must have zero mean value
    dctU = dctn(U, norm='ortho')
    uhat = dctU * iMW
    return(idctn(uhat, norm='ortho'))

```